Medullary thymic epithelial cell depletion leads to autoimmune hepatitis

Anthony J. Bonito,[1] Costica Aloman,[2] M. Isabel Fiel,[3] Nichole M. Danzl,[4] Sungwon Cha,[1] Erica G. Weinstein,[1] Seihwan Jeong,[1] Yongwon Choi,[5] Matthew C. Walsh,[5] and Konstantina Alexandropoulos[1]

[1]Department of Medicine/Clinical Immunology, [2]Department of Medicine/Liver Diseases, and [3]Department of Pathology, Icahn School of Medicine at Mount Sinai, New York, New York, USA. [4]Center for Translational Immunology, Columbia University Medical Center, New York, New York, USA. [5]Department of Pathology and Laboratory Medicine, University of Pennsylvania, Philadelphia, Pennsylvania, USA.

TRAF6, an E3 ubiquitin protein ligase, plays a critical role in T cell tolerance by regulating medullary thymic epithelial cell (mTEC) development. mTECs regulate T cell tolerance by ectopically expressing self-antigens and eliminating autoreactive T cells in the thymus. Here we show that mice with mTEC depletion due to conditional deletion of *Traf6* expression in murine thymic epithelial cells (*Traf6*ΔTEC mice) showed a surprisingly narrow spectrum of autoimmunity affecting the liver. The liver inflammation in *Traf6*ΔTEC mice exhibited all the histological and immunological characteristics of human autoimmune hepatitis (AIH). The role of T cells in AIH establishment was supported by intrahepatic T cell population changes and AIH development after transfer of liver T cells into immunodeficient mice. Despite a 50% reduction in natural Treg thymic output, peripheral tolerance in *Traf6*ΔTEC mice was normal, whereas compensatory T regulatory mechanisms were evident in the liver of these animals. These data indicate that mTECs exert a cell-autonomous role in central T cell tolerance and organ-specific autoimmunity, but play a redundant role in peripheral tolerance. These findings also demonstrate that *Traf6*ΔTEC mice are a relevant model with which to study the pathophysiology of AIH, as well as autoantigen-specific T cell responses and regulatory mechanisms underlying this disease.

Introduction

T cell development and establishment of tolerance to self-antigens occurs in the thymus and depends on cross-talk between thymocytes and the thymic epithelium (1). This cellular compartment is composed of 2 major populations: cortical and medullary thymic epithelial cells (cTECs and mTECs, respectively). Whereas cTECs regulate positive selection of thymocytes and the diversity of the T cell repertoire, mTECs ectopically express tissue-restricted antigens (TRAs) for the purpose of deleting autoreactive T cells that recognize these antigens with high affinity (2–6). In addition, mTECs also affect peripheral tolerance through the production of natural Tregs (nTregs), which suppress aberrant T cell activation in peripheral tissues (7–9). The importance of mTECs in preventing autoimmunity has been revealed through the analysis of genetic mutations that control mTEC development and function in mice and humans (5, 10). In mutant mice, the absence or disruption of the 3-dimensional medullary architecture and defective TRA expression correlates with development of autoimmunity of varied severity, manifested as lymphocyte infiltrates within and autoantibody production against peripheral tissues (11–15). In humans, mutations in the AIRE protein (which controls TRA expression in mTECs) result in autoimmune polyendocrinopathy-candidiasis-ectodermal dystrophy (APECED; also known as autoimmune polyglandular syndrome type 1) (16, 17). This syndrome is characterized by chronic mucocutaneous candidiasis, hypoparathyroidism, and adrenal insufficiency as well as by a higher incidence of diabetes, inflammatory bowel disease, and autoimmune hepatitis (AIH). Thus, proper development of — and antigen presentation by — mTECs plays a key role in the establishment of central tolerance and prevention of autoimmunity.

Existing animal models with mutations that disrupt mTEC development and T cell selection have advanced our understanding of the role of mTECs in induction of central tolerance. However, as most of these mutations also affect the hematopoietic compartment, it is difficult to ascertain the individual contributions of the epithelial versus the hematopoietic compartments to abnormal T cell selection and development of autoimmunity. For example, while members of the TNF receptor superfamily and their corresponding signaling partners have been shown to inhibit TEC development (11, 12, 14, 15), these molecules are also expressed in hematopoietic cells, where they exert their effects in mediating immune responses. In this report, we describe the generation and characterization of conditional knockout mice with deletion of *Traf6* specifically in TECs (*Traf6*ΔTEC mice). These mice developed a T cell–mediated inflammatory response against the liver that exhibited histopathological features of human AIH, representing a novel animal model for the study and treatment of this disease.

Results

TEC-specific deletion of Traf6 inhibits mTEC development. Conditional deletion of *Traf6* in TECs was achieved by crossing floxed *Traf6* mice (18) to animals expressing the *Cre* recombinase under the control of the *foxn1* promoter (ref. 19 and Supplemental Figure 1A; supplemental material available online with this article; doi:10.1172/JCI65414DS1). This gene encodes the transcription factor FOXN1, which regulates thymic epithelial cell development (20). Deletion of *Traf6* expression was confirmed by staining thymic sections with an anti-TRAF6 antibody and the mTEC-specific marker lectin ulex europeous agglutinin–1 (UEA) (21), showing a drastic reduction of TRAF6$^+$UEA$^+$ mTECs in *Traf6*ΔTEC mice (Supplemental Figure 1B). H&E staining of thymic sections revealed diminished medullary areas in *Traf6*ΔTEC mice com-

Conflict of interest: The authors have declared that no conflict of interest exists.
Citation for this article: *J Clin Invest.* 2013;123(8):3510–3524. doi:10.1172/JCI65414.

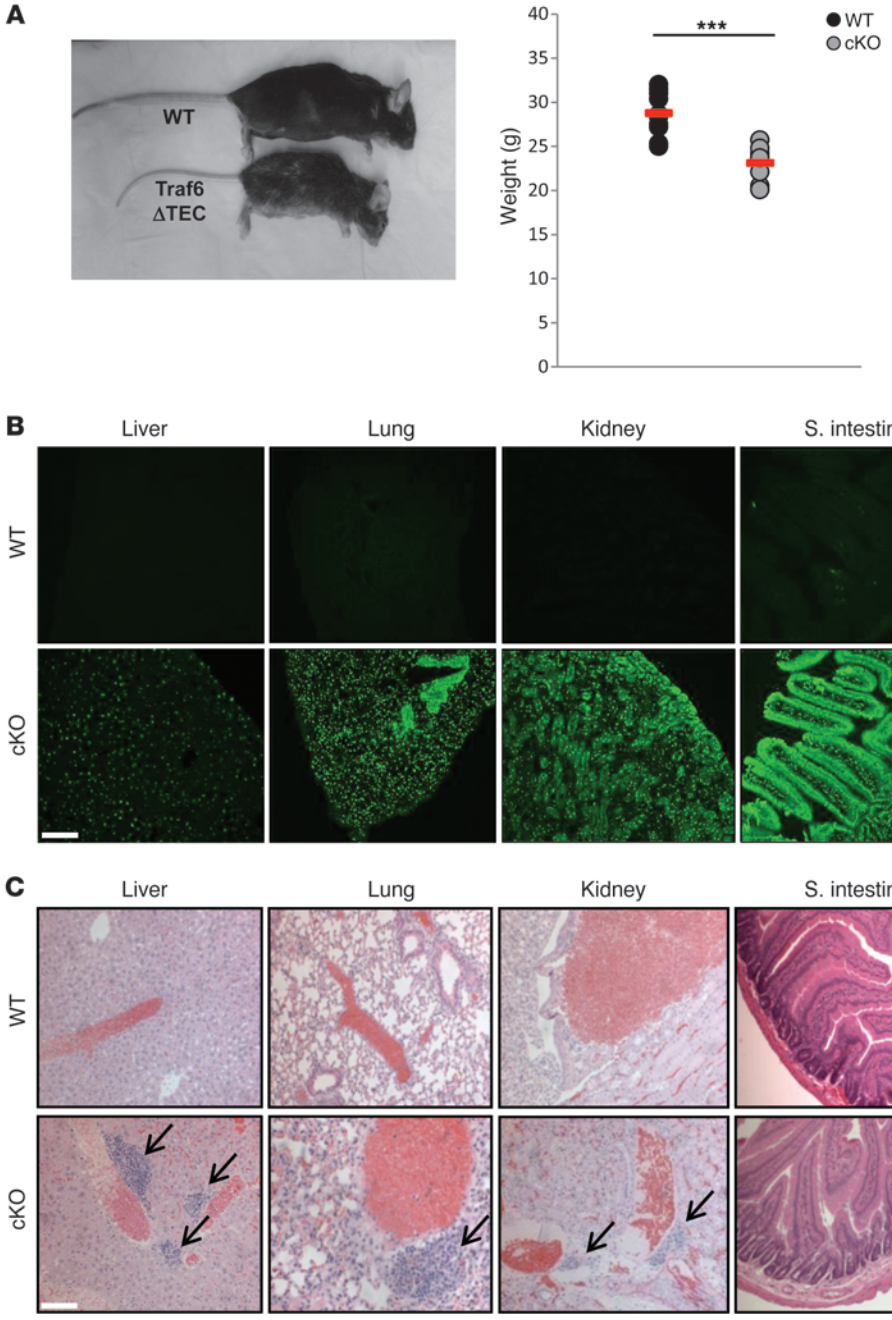

Figure 1

*Traf6*ΔTEC mice develop peripheral autoantibodies and inflammatory infiltrates. (**A**) Images of WT and *Traf6*ΔTEC conditional knockout (cKO) mice. Mouse weight at approximately 6 months of age is also shown. $n = 10$ per genotype. Red bars represent mean. (**B**) Frozen tissue sections from *Rag1*$^{-/-}$ animals (used to eliminate mouse Ig background) were incubated sequentially with sera from 6- to 12-week-old WT or *Traf6*ΔTEC mice, and anti–mouse IgG–FITC and visualized with fluorescence microscopy. (**C**) Paraffin-embedded sections of organs of WT and *Traf6*ΔTEC mice as in **B** were stained with H&E and evaluated for the presence of infiltrates (arrows) by light microscopy. $n \geq 8$ per genotype in **B** and **C**. Scale bars: 200 μm. ***$P < 0.001$.

pared with WT controls (Supplemental Figure 1C). Further, staining of thymic sections with the cortical and medullary markers keratin-8 (K8) and K5, respectively, revealed a marked reduction in K5$^+$ mTECs in *Traf6*ΔTEC mice (Supplemental Figure 2A). The diminished medulla and lack of K5$^+$ mTECs also correlated with markedly reduced UEA$^+$AIRE$^+$ mature mTECs (Supplemental Figure 2A). Quantitative analysis of mTEC subpopulations by flow cytometry showed drastically decreased production of immature and mature mTECs (Supplemental Figure 2B), previously described as UEA$^+$MHCII^{int} and UEA$^+$MHCII^{hi}, or intermediate and mature MHCII^{hi}AIRE$^-$ and MHCII^{hi}AIRE$^+$ cells (22–24). In contrast, cTECs identified as UEA$^-$MHCII$^+$ cells were unaffected

Table 1
Penetrance of autoantibody production and presence of inflammatory infiltrates in young and old WT and *Traf6*ΔTEC mice

Tissue	Young (6–12 weeks)		Old (6–9 months)	
	WT	*Traf6*ΔTEC	WT	*Traf6*ΔTEC
Presence of inflammatory infiltrates				
Liver	0/12	12/12	2/8	8/8
Lung	0/12	6/12	4/8	5/8
Kidney	0/12	4/12	3/8	3/8
Small intestine	0/12	0/12	0/8	1/8
Colon	0/12	0/12	0/8	1/8
Penetrance of autoantibody production				
Liver	0/12	9/12	4/8	7/8
Lung	1/12	10/12	5/8	7/8
Kidney	0/12	9/12	3/8	7/8
Small intestine	0/12	10/11	4/8	8/8
Colon	1/12	10/12	4/8	8/8

The presence of inflammatory infiltrates and autoantibody production in the indicated tissues were determined as described in Figure 1.

by *Traf6* deficiency (Supplemental Figure 2B), consistent with a specific role for TRAF6 in mTEC development. Depletion of mTECs in *Traf6*ΔTEC mice had no apparent effect on thymocyte development, as the total numbers of the different thymocyte populations were comparable to those in WT controls (Supplemental Figure 3A). In addition, mature T cells in the spleen and lymph nodes were unaffected in *Traf6*ΔTEC mice compared with controls (Supplemental Figure 3, B and C). These results showed that TRAF6 is required for, and plays an intrinsic role in, mTEC differentiation, whereas *Traf6* deletion and mTEC depletion has no apparent effect on cTEC and T cell development.

Traf6ΔTEC mice develop AIH. Defects in mTEC development correlate with the presence of peripheral autoimmune manifestations, such as autoantibody production against and presence of inflammatory infiltrates in multiple organs (5, 10). While young *Traf6*ΔTEC mice (6–12 weeks old) appeared healthy, older *Traf6*ΔTEC mice (~6 months old) were smaller compared with WT controls and appeared hunched with ruffled fur (Figure 1A). Despite looking healthy, approximately 80% of young *Traf6*ΔTEC mice developed autoantibodies with reactivity against the liver, lung, kidney, and small and large intestines (Figure 1B and Table 1). Inflammatory infiltrates were also present, but exhibited a more narrow distribution, found predominantly in the liver (100%), and to a lesser extent in the lung (50%) and kidney (33%), of *Traf6*ΔTEC mice (Figure 1C and Table 1). The small intestine and colon appeared normal, despite the presence of autoantibodies against these tissues in the majority of *Traf6*ΔTEC mice (Figure 1C and Table 1). In older *Traf6*ΔTEC animals (6–9 months), the penetrance and distribution of the infiltrates and autoantibodies was similar to that of younger mice, although infiltrates and autoantibodies were also found in some WT mice analyzed (Table 1). Together, these results suggest that the incidence and distribution of autoimmune manifestations in *Traf6*ΔTEC mice appears relatively constant over time, but the phenotype may be compounded as the mice age, which is due to age rather than mTEC depletion–related effects.

Because 100% of the *Traf6*ΔTEC animals examined exhibited liver infiltrates (Table 1), we targeted this organ for further analysis. The hepatic inflammation in older *Traf6*ΔTEC animals was diagnosed as AIH based on several histopathological features typically observed in humans with AIH, including portal inflammation (defined by the presence of inflammatory infiltrates surrounding hepatic portal tracts), interface hepatitis (characterized by infiltrates crossing the limiting plate of inflammation and invading the liver parenchyma), and lobular inflammation (consisting of infiltrates within the liver parenchyma) (Figure 2, A–C). The consequences of chronic hepatic inflammation and tissue damage in *Traf6*ΔTEC mice were reflected by increased collagen deposition and fibrosis surrounding the hepatic vessels and elevated serum alanine aminotransferase (ALT) levels, respectively (Figure 2D). Collagen deposition and fibrosis was quantified by morphometry of picrosirius red–stained, paraffin-embedded liver sections (see Methods and Figure 2D). Analysis of young mice also showed significant differences in AIH histopathology between *Traf6*ΔTEC and WT mice; however, the scores were lower than those of older animals, in which AIH histopathological features peaked at 6 months of age (Supplemental Figure 4).

Traf6ΔTEC mice exhibit classic hallmarks of AIH, such as the presence of plasma cells and anti-nuclear autoantibodies (ANAs). In addition to the histological manifestations discussed above, development of AIH in humans correlates with increased presence of plasma cells in intrahepatic inflammatory lesions as well as elevated total serum Ig levels and organ-specific and non–organ-specific autoantibodies (25–27). To further characterize the AIH phenotype of *Traf6*ΔTEC mice, we assayed for the presence of plasma cells in the liver and the nature of autoantibodies in the serum of these mice. Staining of paraffin-embedded liver sections from *Traf6*ΔTEC and WT mice with the plasma cell–specific dye methyl green-pyronin revealed an increased presence of plasma cells in the portal infiltrates of *Traf6*ΔTEC livers (Figure 3A). A marked increase in the number of $CD138^+$ plasma cells in *Traf6*ΔTEC mice was also found when intrahepatic lymphocyte populations were analyzed by flow cytometry (Figure 3B). This increase in plasma cells, in turn, correlated with ANA presence in *Traf6*ΔTEC mice, as assayed by staining HEp-2 cells with sera from *Traf6*ΔTEC or control animals and determining fluorescence intensity based on arbitrary scores of 1–5 (Figure 3C). The majority of *Traf6*ΔTEC mice (75%) stained positive for ANAs, whereas 20% had autoantibodies against perinuclear proteins and 5% had autoantibodies against both nuclear and cytoplasmic antigens (Figure 3D).

The presence of autoantibodies in *Traf6*ΔTEC mice correlated with a significant increase in total serum Ig and, more specifically, IgG1 and IgM isotype antibody levels (Figure 4, A and B). Western blot analysis of liver extracts showed that autoantibodies in the sera of different *Traf6*ΔTEC animals exhibited similar binding specificities against several liver proteins, whereas sera from WT mice showed limited reactivity (Figure 4C). Both non–organ-specific and organ-specific autoantibodies were present in the sera of *Traf6*ΔTEC mice: some protein bands were present in all tissue extracts, whereas others were unique to the liver (Figure 4D). Together, the presence of plasma cells in the hepatic infiltrates, the increased level of total serum Ig, the presence of ANA, and the organ-specific and non–organ-specific autoantibodies in *Traf6*ΔTEC animals are consistent with the classic features of AIH described in human patients (25–27).

Based on the nature of the autoantibodies present, 2 types of AIH have been identified: type 1, characterized by ANA and/or anti-SMA antibodies; and type 2, characterized by anti–liver and

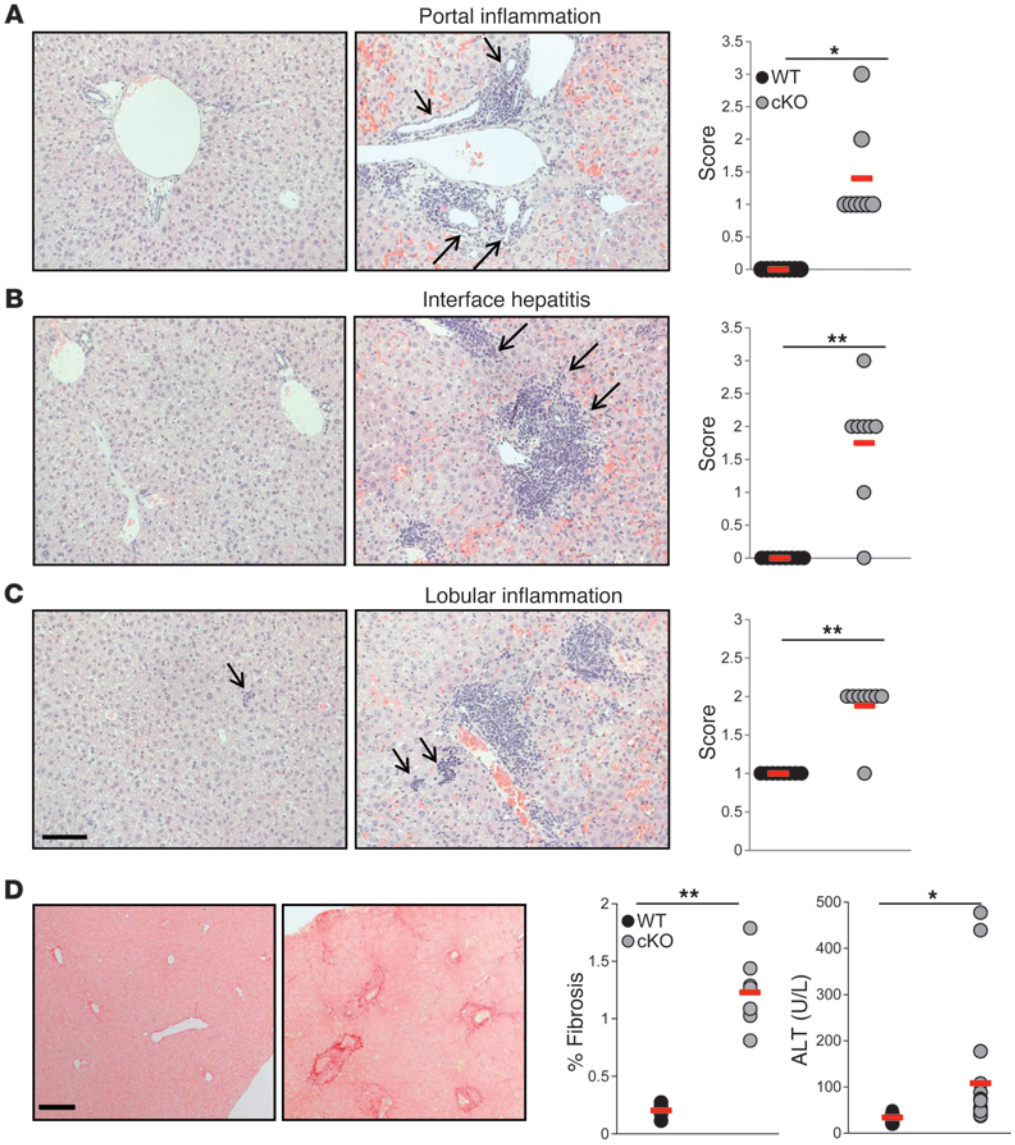

Figure 2
Liver inflammation in *Traf6*ΔTEC mice exhibits pathognomonic features of AIH. (**A**–**C**) Paraffin-embedded liver sections of approximately 6-month-old WT and *Traf6*ΔTEC mice were stained with H&E. Portal inflammation, interface hepatitis, and lobular inflammation (arrows) was scored by a pathologist as described in Methods. (**D**) Picrosirius red staining was used for quantification of liver fibrosis as described in Methods. Serum ALT levels were determined by reflectance spectrophotometry. $n = 8$ per genotype in **A**–**D**. Red bars represent mean. Scale bars: 100 μm (**A**–**C**); 200 μm (**D**). $^{*}P < 0.05$; $^{**}P < 0.01$.

kidney microsomal type 1 (anti-LKM) or anti–liver cytosol type I (anti-LC1) antibodies (26, 28, 29). In addition, anti–soluble liver antigen (anti-SLA) antibodies serve as highly specific serological markers for AIH and exhibit 99% specificity for diagnosing this disease (30–33). Anti-SLA antibodies have been found in 11%–22% of white North American and northern European adult patients with type 1 AIH and are common (18%–44% incidence) in children with type 1 and type 2 AIH (30, 34–36). To further characterize the nature of the autoantibodies in *Traf6*ΔTEC mice, we tested for the presence of anti-SLA, anti-SMA, and anti-LKM autoantibodies. While there was no difference in the levels of anti-SMA and anti-LKM antibodies between *Traf6*ΔTEC and control mice, levels of anti-SLA autoantibodies were significantly increased in *Traf6*ΔTEC mice compared with controls (Figure 4E). We therefore concluded that the presence of ANA and anti-SLA antibodies together in the serum of *Traf6*ΔTEC mice support an AIH phenotype in these animals similar to human type 1 AIH.

Traf6ΔTEC mice exhibit abnormal hepatic T cell populations and T cell function. Since mTECs regulate negative selection of T cells in the thymic medulla (3, 4, 37), and given the observed inflammatory lesions in the liver of *Traf6*ΔTEC mice, we examined whether mTEC depletion correlates with abnormal T cell presence and function in these animals. Costaining frozen liver sections with anti-CD3 and anti-CD4 or anti-CD8 antibodies revealed that the portal infiltrates primarily consisted of $CD3^{+}CD4^{+}$ T cells, whereas $CD3^{+}CD8^{+}$ cells were more prevalent within the liver parenchyma (Figure 5A and data not shown). Further analysis of resident liver T cell populations by flow cytometry confirmed an increase in the total number of $CD4^{+}$ and $CD8^{+}$ T cells in *Traf6*ΔTEC mice compared with WT controls (Figure 5B). In contrast to the liver, we found no significant quantitative or qualitative differences in T cell populations in the spleen and lymph nodes of *Traf6*ΔTEC and control mice (Supplemental Figure 3, B and C, and Supplemental Figure 5B), suggestive of organ-specific, rather than systemic, autoimmunity in *Traf6*ΔTEC animals. Furthermore, analysis of T cells subsets in tissues such as the lung and kidney showed that T cell accumulation was restricted to the liver of *Traf6*ΔTEC mice, as T cell numbers in these tissues were similar to those of

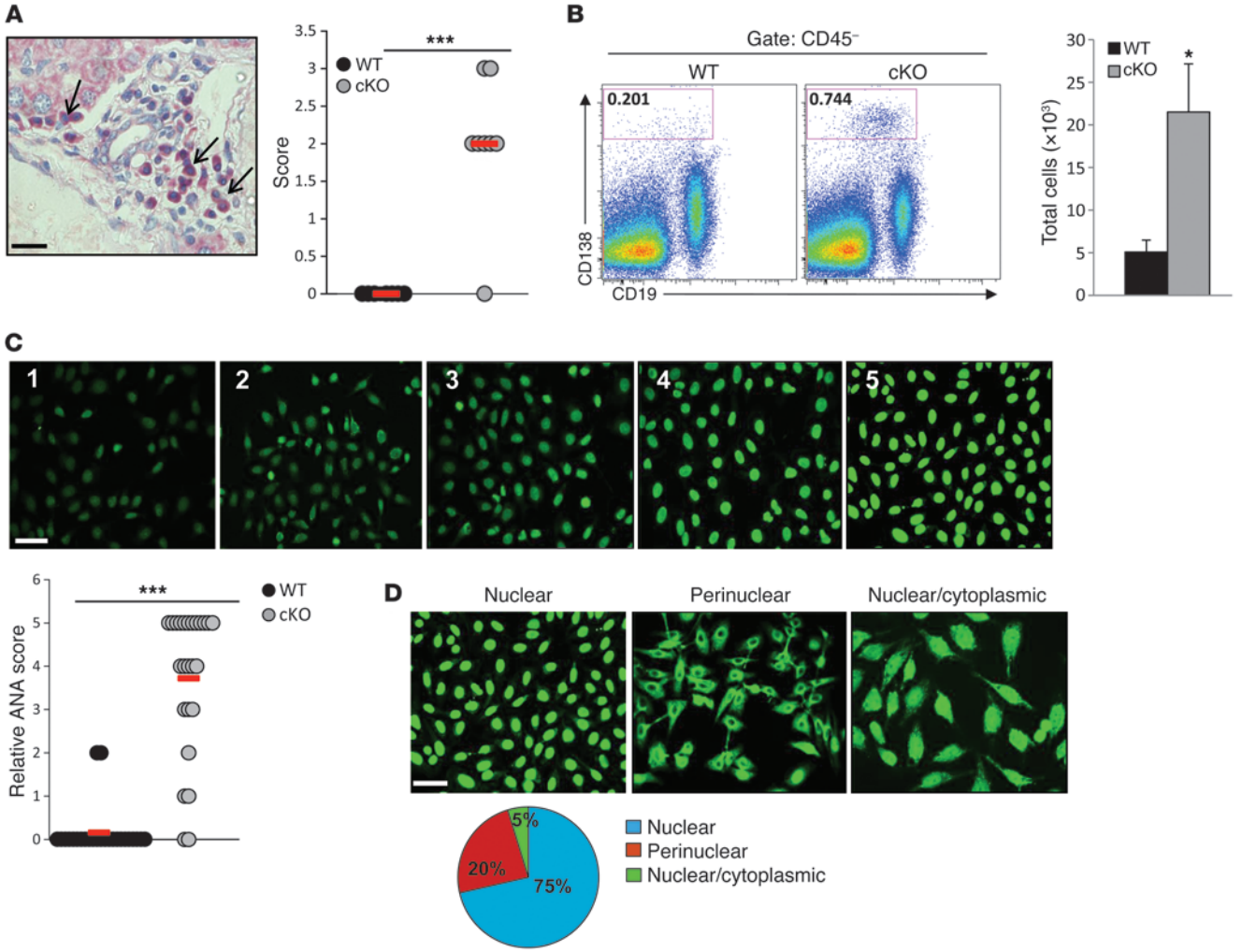

Figure 3

*Traf6*ΔTEC mice exhibit increased numbers of liver plasma cells and elevated serum ANAs. (**A**) Paraffin-embedded liver sections from *Traf6*ΔTEC mice were stained with methyl green-pyronin, and the presence of plasma cells (arrows) was scored as described in Methods. $n = 8$ per genotype. (**B**) Liver cell suspensions from 6- to 8-week-old WT and *Traf6*ΔTEC mice were stained with anti-CD19–eFluor 450 and anti-CD138–biotin/streptavidin PE-Cy7 and analyzed by flow cytometry. $n = 9$ per genotype. Data are pooled results from 3 independent experiments. Bar graph represents mean + SEM. (**C**) Sera of 8- to 10-week-old mice were used to stain HEp-2 cells, and the presence of ANAs was revealed by anti–mouse IgG–FITC and fluorescence microscopy. Data are presented on an arbitrary scale of 1–5, based on HEp-2 cell staining and ANA fluorescence intensity. $n = 25$ per genotype. Data are pooled results from at least 3 independent experiments. Red bars represent mean. (**D**) Representative patterns of autoantibody staining and frequency within the sample population shown in **C**. Scale bars: 20 μm (**A**); 40 μm (**C** and **D**). $^*P < 0.05$; $^{***}P < 0.001$.

controls (Supplemental Figure 5, A, C, and D). In addition to increased numbers of $CD4^+$ and $CD8^+$ T cell subsets, an aberrant $CD4^+CD8^+$ double-positive population of T cells was markedly increased in the liver of *Traf6*ΔTEC mice, but not in other tissues (Figure 5B and Supplemental Figure 5). $CD4^+CD8^+$ cells have been identified in peripheral blood of patients with autoimmune diseases and are thought to have escaped thymic selection (38, 39). Therefore, it is possible that the presence of such cells in the liver of *Traf6*ΔTEC mice corresponds to abnormal thymic selection of T cells due to the observed mTEC depletion. Alternatively, as $CD4^+CD8^+$ T cells have been shown to represent peripherally hyperactivated T cells in animals and humans (40, 41), their presence in the liver may result from the inflammation induced in this organ by mTEC depletion.

Further analysis of *Traf6*ΔTEC and WT liver T cells revealed that CD44 and CD69 expression increased 3-fold in the *Traf6*ΔTEC $CD4^+$ T cell subset and 6-fold in the *Traf6*ΔTEC $CD8^+$ T cell subset compared with controls (Supplemental Figure 6, A and B), suggesting an activated phenotype for these cells. In contrast, and although activated T cells subsets were found in the spleen and, to a lesser extent, the lung and kidney of *Traf6*ΔTEC mice, the increase was <1-fold compared with WT controls (Supplemental Figure 6, A and B). These results were consistent with the low prevalence and distribution of infiltrates in the lung and kidney of *Traf6*ΔTEC animals compared with widespread infiltration in the liver. These data also suggest targeted homing of T cells to the liver of *Traf6*ΔTEC mice, as opposed to sequestration of activated T cells from the periphery. In support of targeted sequestration, perfusion of the liver prior to

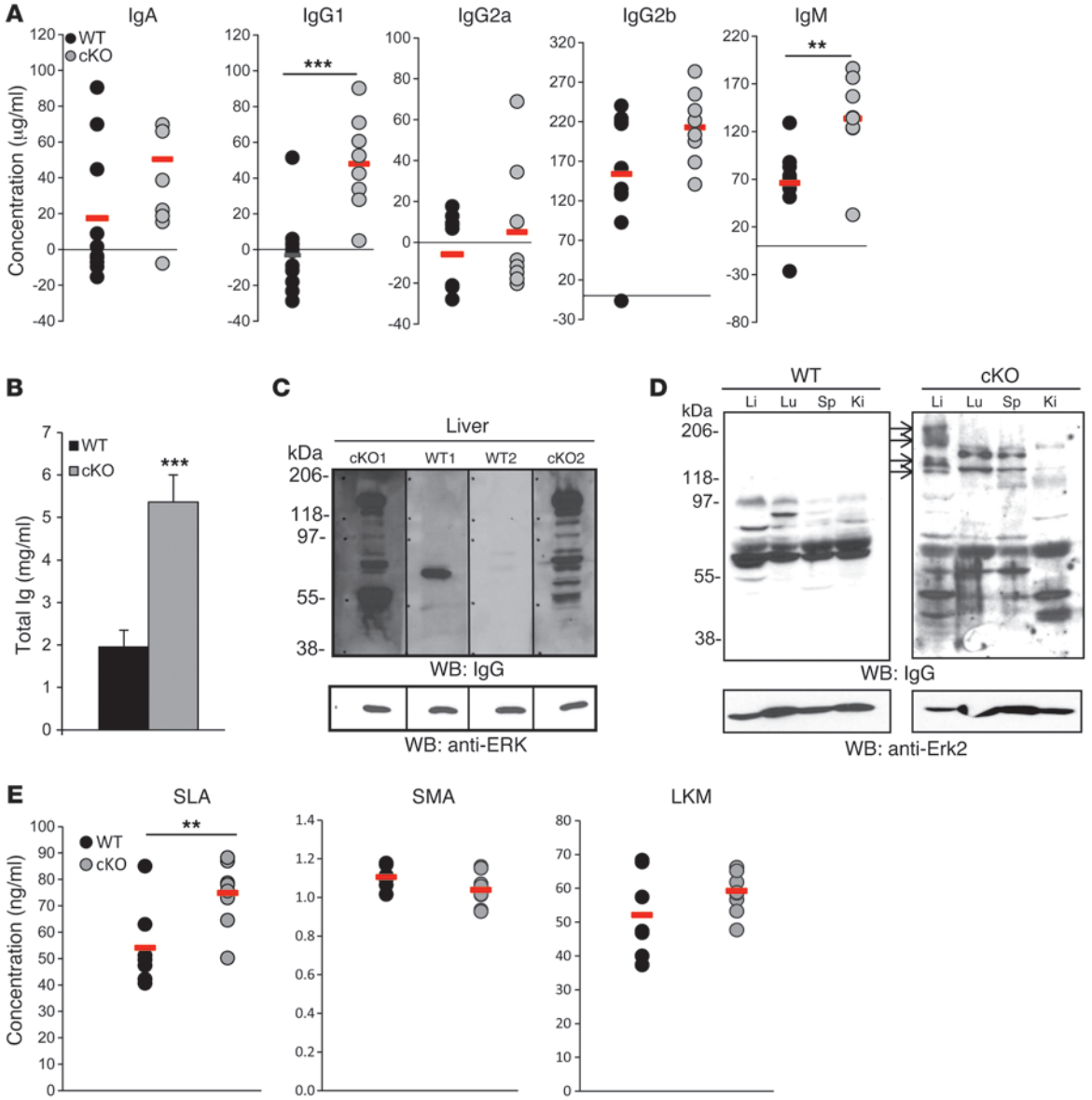

Figure 4

*Traf6*ΔTEC mice produce autoantibodies that bind to liver-specific proteins. (**A** and **B**) Concentrations of different antibody isotypes (**A**) and total Ig (**B**) in the sera of 6- to 12-week-old WT and *Traf6*ΔTEC mice were determined by ELISA. $n \geq 8$ per genotype. Data are pooled results from 3 independent experiments run in triplicates. Red bars represent mean. Bar graph represents mean + SEM. (**C** and **D**) Western blots of normal tissue lysates (100 μg) from *Rag1*$^{-/-}$ mice were incubated with sera (1:100) from WT and *Traf6*ΔTEC mice as shown, followed by horseradish peroxidase–conjugated anti–mouse IgG secondary antibody. Protein bands in **C** and **D** were visualized by chemiluminescence as described in Methods. Blots were stripped and reprobed with anti-Erk antibody (loading control). In **C**, blots were cut apart in order to be incubated with different sera, then reassembled (black lines). Arrows in **D** denote protein bands that are unique to the liver. Representative blots from 1 of at least 2 independent experiments are shown. Li, liver; Lu, lung; Sp, spleen; Ki, kidney. (**E**) Autoantibody concentrations in the sera of 6- to 12-week-old WT and *Traf6*ΔTEC mice, determined by ELISA. $n \geq 7$ per genotype. Red bars represent mean. $^{**}P < 0.01$; $^{***}P < 0.001$.

T cell isolation and the finding that T cell subsets in the blood of *Traf6*ΔTEC mice were composed entirely of naive ($CD62^+CD44^-$) T cells (Supplemental Figure 6C) argue against recruitment of activated T cells into the liver from circulating blood.

Although the trigger for human AIH is currently unknown, existing evidence suggests that disrupted immune homeostasis plays a permissive role in disease development. Liver damage is thought to be mediated by autoreactive $CD4^+$ T cells that recognize and respond to liver-specific peptide(s) (26, 42). Given that mTECs regulate elimination of autoreactive T cells in the thymus and the presence of activated T cells in the liver of *Traf6*ΔTEC mice, we examined whether liver T cells respond to liver APCs in syngeneic mixed lymphocyte reactions. We found significantly increased proliferation of *Traf6*ΔTEC liver T cells compared with controls in response to syngeneic APC stimulation (Figure 5C); in contrast, these cells responded to the same extent when

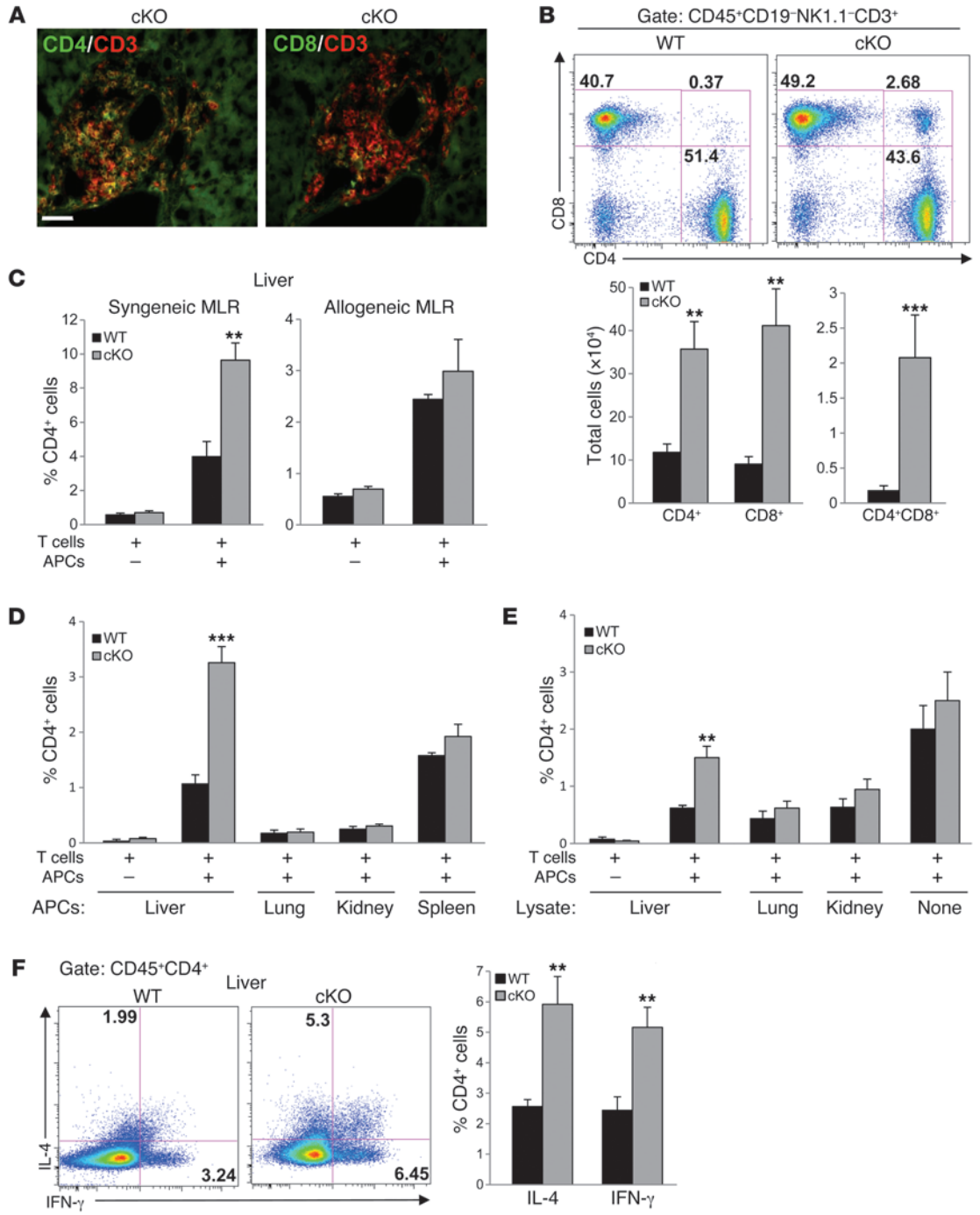

Figure 5

Abnormal T cell presence and immune responses in the liver of *Traf6*ΔTEC mice. (**A**) Staining of frozen liver sections from *Traf6*ΔTEC mice with anti-CD3 and anti-CD4 or anti-CD8 antibodies showed increased presence of $CD3^+CD4^+$ T cells in hepatic portal tracts. (**B**) Total T cell population numbers were quantified by flow cytometry in liver hematopoietic cell suspensions from WT and *Traf6*ΔTEC mice stained with different antibodies. $n = 8$ per genotype. (**C**) Liver T cells purified from WT or *Traf6*ΔTEC mice were stained with CFSE, then incubated with liver syngeneic (C57BL/6) or allogeneic (Balb/c) $CD11c^+$ APCs in vitro for 72 hours. Percent CFSE-labeled $CD4^+$ cells was determined by flow cytometry. $n = 7$ per genotype, run in triplicates. MLR, mixed lymphocyte reaction. (**D**) CFSE-labeled liver T cells were incubated 1:1 with syngeneic $CD11c^+$ APCs purified from the indicated tissues. 72 hours later, percent $CD4^+CFSE^+$ T cells was determined by flow cytometry. $n = 6$, run in triplicates. Data are pooled results from 2 independent experiments. (**E**) CFSE-labeled liver T cells were incubated 1:1 with GM-CSF bone marrow–derived DCs unloaded or loaded with the indicated lysates for 5 days. Percent $CD4^+CFSE^+$ T cells was analyzed by flow cytometry. $n = 9$ per genotype, run in triplicates. Data are pooled from 3 independent experiments. (**F**) Intracellular staining of purified WT and *Traf6*ΔTEC liver T cells was performed with anti–IL-4–PE and anti–IFN-γ–allophycocyanin antibodies and flow cytometry. $n = 8$ per genotype. Bar graphs represent mean + SEM. Scale bar: 50 μm. $^{**}P < 0.01$; $^{***}P < 0.001$.

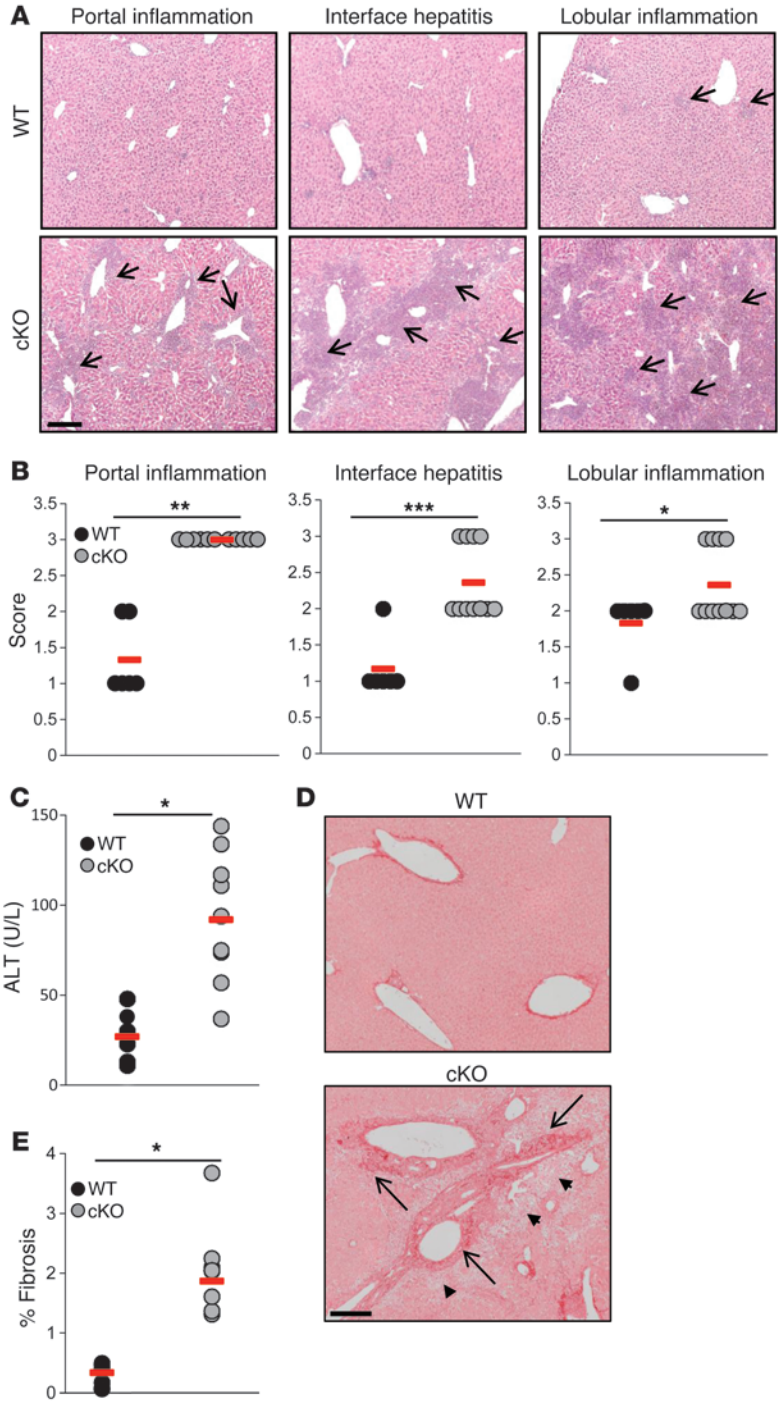

Figure 6

Transfer of *Traf6*ΔTEC liver T cells in immunodeficient recipients results in development of AIH. (**A** and **B**) Liver CD3$^+$ T cells purified from WT and *Traf6*ΔTEC mice were injected into *Rag1*$^{-/-}$ mice. Paraffin-embedded, H&E-stained liver sections of recipient animals were analyzed 4–6 weeks after transfer for the presence of infiltrates (arrows). For histopathologic parameters used to define AIH, see Methods and Figure 2. (**C**) ALT levels in the sera of *Rag1*$^{-/-}$ recipients of WT or *Traf6*ΔTEC liver T cells, indicative of tissue damage, were determined as described in Methods. (**D** and **E**) Fibrosis (arrows) due to collagen deposition was quantified by picrosirius red staining, as described in Methods and Figure 2. Arrowheads indicate tissue damage around fibrotic vessels, known as hepatocyte dropout areas. Liver CD3$^+$ T cells from 8-week-old WT and *Traf6*ΔTEC mice were transferred into an equal number of recipient *Rag1*$^{-/-}$ mice in these experiments. $n \geq 6$ per genotype. Data in **A**–**E** are pooled results from 3 independent transfer experiments. Red bars represent mean. Scale bars: 200 μm. $^*P < 0.05$; $^{**}P < 0.01$; $^{***}P < 0.001$.

stimulated with allogeneic APCs or anti-CD3/CD28 antibodies (Figure 5C and data not shown), which suggests that there were no inherent defects in the ability of WT cells to proliferate. In addition, consistent with normal peripheral responses in *Traf6*ΔTEC animals, WT and *Traf6*ΔTEC splenic T cells responded similarly to syngeneic or allogeneic stimulation (Supplemental Figure 7A). The specificity of liver *Traf6*ΔTEC T cells for liver APC/antigen complexes was further assessed by incubating liver T cells from WT and *Traf6*ΔTEC animals with syngeneic APCs isolated from different organs. Whereas *Traf6*ΔTEC liver T cells responded robustly to liver APCs compared with controls, these cells failed to proliferate when stimulated with APCs isolated from the lung or kidney of the same animals and responded similarly to WT T cells when stimulated with splenic APCs (Figure 5D). Furthermore, when the specificity of *Traf6*ΔTEC liver T cells for liver antigens was tested using in vitro–differentiated APCs loaded with cell extracts from different tissues, we found a significant increase in *Traf6*ΔTEC liver T cell proliferation in response to stimulation with liver extracts, but not lung or kidney extracts (Figure 5E). The proliferation of *Traf6*ΔTEC liver T cells under these conditions exhibited longer kinetics as well as a lower level of activation than those observed with liver-derived APCs (Figure 5D), likely reflecting the rarity of autoreactive T cells responding to liver antigens. In contrast, similar to the results with splenic APCs (Figure 5D), there was no significant difference in the proliferation of WT versus *Traf6*ΔTEC liver T cells when these were stimulated with unloaded APCs (Figure 5E), which suggests that both types of cells respond to endogenous antigens to a similar extent. Collectively, these results suggest that mTEC depletion in the thymus results in the production of autoreactive T cell clones that home predominantly to the liver of *Traf6*ΔTEC mice, where they bind and respond to liver antigens and promote the development of inflammatory lesions and AIH.

As mentioned above, liver damage associating with AIH development is thought to be mediated by autoreactive CD4$^+$ T cells that recognize and respond to liver-specific peptides. Once activated, Th0 cells differentiate into Th1 cells secreting IFN-γ, an important intermediary in tissue destruction, and/or into Th2 cells, which produce IL-4, IL-10, and IL-13 cytokines and promote antibody production by plasma cells (26, 42). Consistent with this model, we found significantly increased numbers of IFN-γ– and IL-4–produc-

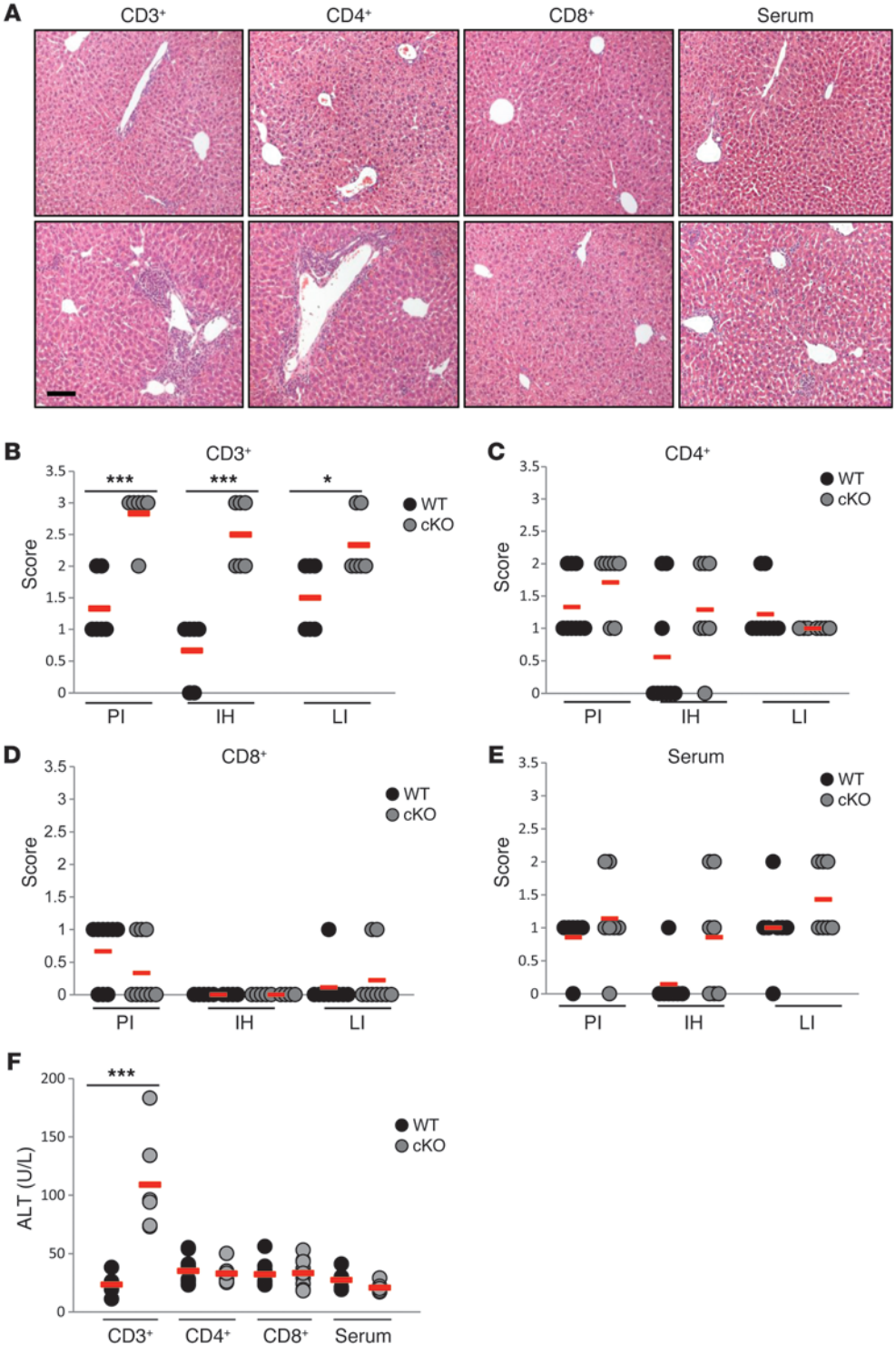

Figure 7

Development of AIH requires the contribution of more than 1 lymphocyte cell subset. (**A**–**E**) Sorted liver CD3+, CD4+, and CD8+ T cells and sera purified from 8-week-old WT and *Traf6*ΔTEC mice were injected into an equal number of *Rag1*$^{-/-}$ mice. Paraffin-embedded and H&E-stained liver sections of recipient animals were analyzed approximately 6 weeks after transfer for the presence of infiltrates. (**F**) ALT levels in the sera of *Rag1*$^{-/-}$ recipients adoptively transferred with liver WT or *Traf6*ΔTEC T cells or sera, determined as described in Figure 6 and Methods. $n \geq 6$ per genotype in all transferred groups. Data in **A**–**E** are pooled results from 3 independent transfer experiments. PI, portal inflammation; IH, interface hepatitis; LI, lobular inflammation. Red bars represent mean. Scale bar: 100 μm. *$P < 0.05$; ***$P < 0.001$.

ing cells and, to a lesser extent, IL-17–producing cells in the liver of *Traf6*ΔTEC versus WT mice (Figure 5F and data not shown), whereas normal numbers of cells producing these cytokines were found in the spleens of the same animals (Supplemental Figure 7B). Similarly, we found no difference in serum Th1, Th2, Th17, or inflammatory cytokine levels between *Traf6*ΔTEC and control mice (Supplemental Figure 7C), consistent with normal systemic immune responses in *Traf6*ΔTEC animals. Thus, the T cell–containing infiltrates in the liver of *Traf6*ΔTEC mice exhibit an effector T cell phenotype that recapitulates that observed in human AIH and may be driving chronic liver damage and fibrosis in these mice.

Transfer of liver T cells from Traf6ΔTEC donors into immunodeficient mice leads to AIH development. One hallmark of autoimmune disease is the ability of immune cells to adoptively transfer the disease to another host. To determine whether the T cells present in the liver of *Traf6*ΔTEC animals were able to promote AIH develop-

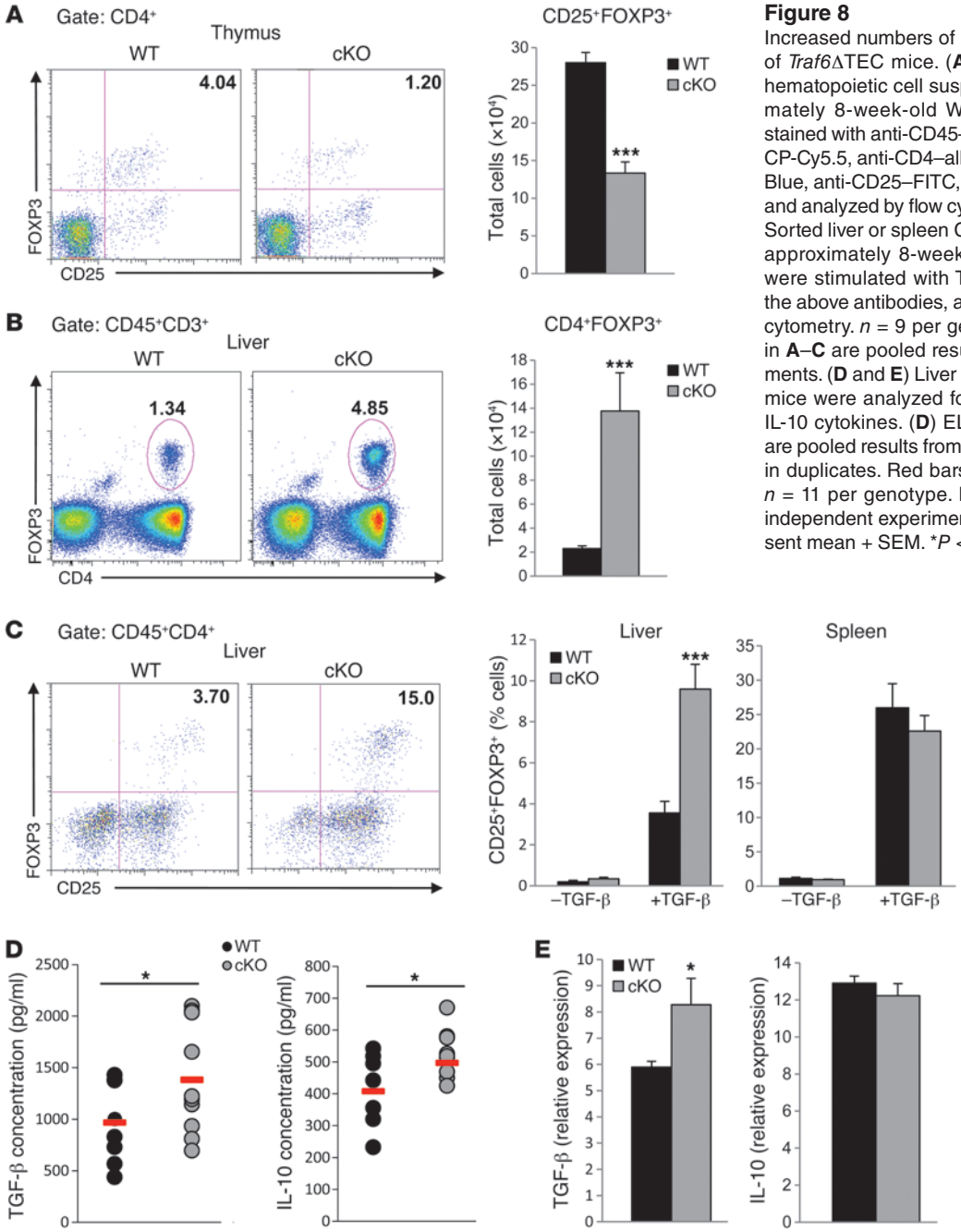

Figure 8

Increased numbers of iTregs and cytokines in the liver of *Traf6*ΔTEC mice. (**A** and **B**) Thymocytes and liver hematopoietic cell suspensions isolated from approximately 8-week-old WT and *Traf6*ΔTEC mice were stained with anti-CD45–Alexa Fluor 750, anti-CD3–PerCP-Cy5.5, anti-CD4–allophycocyanin, anti-CD8–Pacific Blue, anti-CD25–FITC, and anti-FOXP3–PE antibodies and analyzed by flow cytometry. $n = 9$ per genotype. (**C**) Sorted liver or spleen CD4$^+$CD25$^-$ T cells isolated from approximately 8-week-old WT and *Traf6*ΔTEC mice were stimulated with TGF-β in vitro and stained with the above antibodies, and iTregs were analyzed by flow cytometry. $n = 9$ per genotype, run in triplicates. Data in **A**–**C** are pooled results from 3 independent experiments. (**D** and **E**) Liver lysates from WT and *Traf6*ΔTEC mice were analyzed for the production of TGF-β and IL-10 cytokines. (**D**) ELISA. $n \geq 7$ per genotype. Data are pooled results from 2 independent experiments run in duplicates. Red bars represent mean. (**E**) RT-PCR. $n = 11$ per genotype. Data are pooled results from 2 independent experiments run in triplicates. Bars represent mean + SEM. $^*P < 0.05$; $^{***}P < 0.001$.

ment, sorted liver CD3$^+$ T cells were adoptively transferred into *Rag1*$^{-/-}$ recipient mice. *Rag1*$^{-/-}$ recipients of *Traf6*ΔTEC liver T cells developed AIH of increased severity compared with the donor mice (Supplemental Figure 8) and with the mice analyzed in Figure 2. Portal and lobular inflammation and interface hepatitis were all significantly increased in *Rag1*$^{-/-}$ recipients of *Traf6*ΔTEC versus WT liver T cells and compared with donor mice (Figure 6, A and B, and Supplemental Figure 8, A and B). The hepatic inflammation correlated with significantly increased levels of ALT in recipients of *Traf6*ΔTEC liver T cells compared with WT controls and donor mice (Figure 6C and Supplemental Figure 8C). Liver fibrosis was also significantly increased in *Rag1*$^{-/-}$ recipients of *Traf6*ΔTEC liver T cells, with evident tissue damage shown as hepatocyte dropout areas around fibrotic vessels (Figure 6, D and E). The fibrosis was more severe than in *Traf6*ΔTEC mice (compare Figure 6D and Figure 2D), whereas minimal fibrosis was observed in *Rag1*$^{-/-}$ mice receiving WT liver T cells (Figure 6, D and E). Some *Rag1*$^{-/-}$ recipient animals developed colitis regardless of the nature of the donor cells (data not shown), which suggests that liver T cells exhibit colitogenic properties. In contrast, transfer of splenic T cells or total splenocytes isolated from the same mice failed to promote disease development in *Rag1*$^{-/-}$ recipients (data not shown). Together, these data suggest that *Traf6* deletion in TECs and mTEC depletion associates with organ-specific rather than systemic autoim-

munity and that production of aberrant liver T cell populations is responsible for AIH development in *Traf6*ΔTEC mice.

To further determine whether a specific T cell subpopulation is responsible for AIH transfer in *Rag1*$^{-/-}$ recipients, we performed adoptive transfers of sorted T cell subsets from WT and *Traf6*ΔTEC mice. Total CD3$^+$ T cell transfers from different mice were included in these experiments as positive controls (Figure 7, A and B). Transfer of *Traf6*ΔTEC CD4$^+$ T cells led to accumulation of infiltrates in hepatic portal tracks in the majority of recipient *Rag1*$^{-/-}$ mice (Figure 7A). However, the histopathological scores of AIH in these recipients were not significantly different from those of mice adoptively transferred with WT cells (Figure 7C). On the other hand, transfer of CD8$^+$ cells sorted from the same mice failed to promote infiltrate formation or significant differences in AIH scores in the majority of the recipient animals (Figure 7, A and D). Similar to CD4$^+$ T cells, transfer of serum from *Traf6*ΔTEC and WT mice into *Rag1*$^{-/-}$ recipients led to some infiltrate formation, but again, no significant differences were observed in the histopathological AIH scores of the different recipients (Figure 7, A and E). In these experiments, we also attempted to transfer CD4$^+$CD8$^+$ T cells; however, we failed to purify enough cells from several mice, as these cells were exceedingly rare, especially in WT mice. Therefore, the ability of the CD4$^+$CD8$^+$ cells to transfer the disease could not be assessed. Finally, analysis of ALT levels of the different recipient mice was consistent with their histopathological scores: increased ALT levels were observed only in recipients of total *Traf6*ΔTEC CD3$^+$ T cells, not in recipients of T cell subsets (Figure 7F). These results suggest that although liver T cells are important for disease development in *Traf6*ΔTEC mice, a complex interplay among different T cell subsets, and likely B cells, is required for disease development. Thus, CD4$^+$ T cells may be responsible for initiating the inflammatory response in an antigen-specific manner, whereas other T cell subsets and/or B cells play a secondary/complimentary role in disease development.

Traf6ΔTEC mice exhibit normal peripheral tolerance, despite reduced thymic output of nTregs. In addition to regulating the negative selection of autoreactive T cells, mTECs have also been shown to regulate production of nTregs in the thymus (7–9). Because a reduction in the numbers and/or functional impairment of Tregs is thought to correlate with AIH development (43, 44) and because Tregs are potent suppressors of inflammation and autoimmunity, we next examined whether Treg production and function is impaired in *Traf6*ΔTEC mice. Staining of thymocyte cell suspensions with the Treg-specific marker FOXP3 revealed a 50% decrease in the total number of FOXP3$^+$ thymocytes (Figure 8A), consistent with a role for mTECs in nTreg production. However, there was no difference in the number of splenic FOXP3$^+$ T cells between *Traf6*ΔTEC and WT mice, and *Traf6*ΔTEC CD25$^+$FOXP3$^+$ splenic T cells were equally able to suppress T effector function in vitro compared with WT controls (Supplemental Figure 9, A and B). On the other hand, we found a marked increase in the number of FOXP3$^+$ T cells in *Traf6*ΔTEC versus WT liver (Figure 8B). The increase in cell numbers correlated with increased production of induced CD25$^+$FOXP3$^+$ Tregs (iTregs) when *Traf6*ΔTEC CD4$^+$CD25$^-$ liver T cells were incubated with TGF-β in vitro (Figure 8C). In contrast, and consistent with the normal numbers of CD25$^+$FOXP3$^+$ Tregs in the spleen of *Traf6*ΔTEC mice (Supplemental Figure 9A), we observed no difference in the percentage of iTregs when splenic *Traf6*ΔTEC or WT CD4$^+$CD25$^-$ T cells were similarly stimulated in vitro (Figure 8C). Consistent with the in vitro production of iTregs, we found significantly increased protein and RNA levels of TGF-β and IL-10 in liver extracts from *Traf6*ΔTEC animals compared with controls (Figure 8, D and E). Thus, despite the decreased thymic output of nTregs, peripheral mechanisms such as homeostatic expansion of nTregs in the spleen and/or inflammation-driven production of iTregs in the liver of *Traf6*ΔTEC mice may compensate for the reduced nTreg thymic output in these animals.

Discussion

In this report, we examined the role of impaired mTEC development on T cell–mediated autoimmunity within the context of a normal hematopoietic cell compartment, which provided a unique opportunity to decipher the mechanisms of mTEC differentiation and central tolerance. Peripheral T cell subsets and T cell immune responses were normal in *Traf6*ΔTEC mice, supporting organ-specific (rather than systemic) development of autoimmunity. Consistent with this, and although the majority of *Traf6*ΔTEC mice developed autoantibodies against most of the tissues tested, the distribution of inflammatory lesions was largely restricted to the liver — and, to a lesser extent, the lung and kidney — of these mice. The reduced prevalence or absence of infiltrates in nonhepatic tissues was not due to different kinetics of autoimmunity development, as the incidence of inflammatory infiltrates in the different organs was similar between young and older animal cohorts. In addition, the reduction or lack of T cell–containing infiltrates in tissues other than the liver was not due to altered (patchy or diffuse) distribution of immune cells, as quantification of total T cells from the spleen, lung, and kidney of several mice revealed similar numbers of T cells between WT and *Traf6*ΔTEC animals. This was in contrast to the liver, where we found large increases in the total numbers of both CD4$^+$ and CD8$^+$ T cells. Given the presence of autoantibodies in the serum and inflammatory infiltrates in the lung and kidney of some *Traf6*ΔTEC mice, we currently cannot exclude the possibility that these effects also contribute to the overall disease phenotype in *Traf6*ΔTEC animals. Nonetheless, our results showing (a) complete penetrance of liver inflammation in all *Traf6*ΔTEC animals tested; (b) increased numbers of total and activated/autoreactive T cells in *Traf6*ΔTEC liver compared with other tissues; (c) stimulation of *Traf6*ΔTEC liver T cell proliferation by liver, but not by other APCs, and by APCs loaded with liver cell extracts, but not lung and kidney extracts, and (d) the presence of anti-SLA and other liver-specific autoantibodies in the serum of *Traf6*ΔTEC mice suggest that the liver is targeted in these mice by autoreactive T cells that escape deletion in the thymus due to mTEC depletion.

It is currently unclear why the liver is the organ predominantly affected in *Traf6*ΔTEC mice, as expression of all peripheral antigens in mTECs should be similarly affected by mTEC depletion. As different TRAs are stochastically expressed in mTECs (45), it is possible that autoimmune manifestations vary in a manner dependent on the genetic background of the animals, or the nature of the genetic mutation resulting in mTEC depletion. In terms of genetic background, whereas inflammation was mostly contained within the liver in C57BL/6 mice, we observed a wider range of phenotypes affecting different tissues, including the skin, eye, joints, and muscle, in a mixed (129/SvJ/C57BL/6) genetic background. It is possible that mTEC depletion by *Traf6* deletion in a more permissive, autoimmune-prone background may reveal a wider spectrum of autoimmune manifestations than in the current mouse model. In terms of the genetic mutations used to deplete mTECs,

the phenotype of *Traf6*ΔTEC mice was in sharp contrast to previous experiments with straight *Traf6* knockout mice and other models with defective mTEC development. In *Traf6*ΔTEC mice, TEC-specific deletion of *Traf6* correlates with chronic inflammation, and despite looking unhealthy, the mice survive for at least 1 year after birth. In contrast, in straight knockout mouse models with mutations affecting proteins that regulate the noncanonical NF-κB pathway and mTEC development (including TRAF6), mTEC depletion in homozygous mice correlated not only with peripheral autoimmune manifestations, but also early lethality (12). In those animal models, the hematopoietic compartment was also shown to contribute to autoimmunity development and reduced survival, as the affected proteins were expressed in both the epithelial and the hematopoietic compartments. Autoimmune manifestations in these mice were more pronounced and led to early death due to systemic effects and lymphoproliferation, effects that are absent in *Traf6*ΔTEC mice, in which the hematopoietic compartment is intact. Consistent with this, T cell–specific deletion of *Traf6* (*Traf6*ΔT mice) led to multiorgan inflammatory disease and lymphadenopathy due to defective Treg-mediated suppression of *Traf6*ΔT T cell responses (46). Despite the differences in survival between existing models and our *Traf6*ΔTEC mouse, liver inflammation has been found in all animals with mTEC defects; however, a connection to AIH had not previously been established. Therefore, the extended lifespan of the *Traf6*ΔTEC mice, together with the chronic, organ-specific (instead of systemic) nature of the inflammation, makes these animals an attractive and convenient model with which to study AIH.

The chronic nature of liver inflammation in *Traf6*ΔTEC mice correlated with increased presence of FOXP3$^+$ T cells in the liver of these animals. Therefore, despite the reduced thymic nTreg output in *Traf6*ΔTEC animals, the normal presence and function of the peripheral Treg compartment, the increased frequency of iTregs, and the increased levels of TGF-β and the immunosuppressive cytokine IL-10 in the liver of *Traf6*ΔTEC mice may all be responsible for their lack of overt peripheral T cell responses and the chronic nature of their hepatic inflammation. A correlation between reduced Treg numbers and/or functional impairment of Tregs and development of AIH has been observed in human patients (26). However, a recent report showed that the numbers and suppressive function of FOXP3$^+$ T cells isolated from AIH patients were similar to those of normal controls. In addition, the intrahepatic frequency of these cells was higher and correlated with the degree of inflammation in the liver of AIH patients (47). Our results support the latter observations and suggest that in *Traf6*ΔTEC mice, inflammation-driven production of iTregs in the liver may compensate for the reduced nTreg thymic output and drive the chronic nature of the disease. Consistent with this, existing evidence supports a protective role for iTregs in established or induced autoimmunity in several mouse models (48, 49).

The liver inflammation and AIH development in *Traf6*ΔTEC mice is quite intriguing, given that the liver is considered a privileged organ from an immunological standpoint. It is well known that transplanted livers are less frequently rejected than other solid organ transplants (50–53). In addition, liver autoimmune diseases like AIH develop with lower frequency compared with other autoimmune conditions, for example, type 1 diabetes and multiple sclerosis (54). Although the causes of AIH remain unknown, current models of AIH development propose that hepatitis development and ensuing tissue damage is orchestrated by naive CD4$^+$ T lymphocytes recognizing liver self-peptides. Following antigen binding, activated CD4$^+$ Th0 cells differentiate into IFN-γ–secreting Th1 cells that activate macrophages and increase MHCI expression on hepatocytes, rendering liver cells susceptible to CD8$^+$ T cell–mediated cytotoxicity. Th0 cells can also differentiate into Th2 effector cells that secrete IL-4, IL-10, and IL-13 cytokines, favoring autoantibody production by plasma cells (26, 42). The major components of this model were recapitulated in the *Traf6*ΔTEC mice, shown by increased total numbers of CD4$^+$ and CD8$^+$ T cells, increased production of both Th1 and Th2 cytokines, and increased presence of plasma cells and autoantibody production. In addition, our results showing that individual T cell subsets failed to recapitulate AIH development in recipient mice further supported the idea that complex interplay among lymphocyte cell subsets is required for disease development, with self-antigen recognition by autoreactive CD4$^+$ T cells playing a key role in disease initiation. Consistent with this, susceptibility of human patients to AIH has been linked to deviant DRB1 alleles within the human leukocyte antigen (HLA) region (55–57). As these molecules present peptide antigens to CD4$^+$ T cells, compromised antigen presentation by susceptibility alleles and recognition of liver self-antigens by naive T lymphocytes is thought to contribute to AIH pathogenesis. A similar mechanism may be in effect in *Traf6*ΔTEC mice, as antigen presentation was indeed compromised by mTEC depletion in these animals. In addition, our observation of anti-SLA autoantibodies present in the sera of *Traf6*ΔTEC mice supports faulty antigen presentation in these mice, as anti-SLA autoantibody production has been linked to HLA DRB1*0301 alleles (33, 58), which, together with DRB1*0401 alleles, are the principal genetic risk factors for development of type 1 AIH in certain patients (30, 34–36).

Finally, impaired antigen presentation due to mTEC depletion and elimination of autoreactive T cells in *Traf6*ΔTEC mice may mimic or replicate the conditions that promote pathogenesis of AIH in humans in different disease settings. The observation that 10%–15% of patients with APECED (the result of impaired AIRE function and antigen expression in mTECs) develop AIH (59, 60) provides further support for impaired antigen presentation and mTEC function in the pathogenesis of AIH. Therefore, despite the existence of several mouse models of AIH involving chemically induced or liver-intrinsic perturbations of hepatic immune responses (25, 54, 61), we believe that the *Traf6*ΔTEC mouse represents a relevant model by which to study the pathogenic mechanisms leading to development of this disease and explore new therapeutic approaches. Further characterization of the *Traf6*ΔTEC mouse model can not only improve our understanding of the pathophysiology of AIH, but may also lead to a broader understanding of how liver tolerance is established and maintained, with wider impact on other liver autoimmune diseases and liver transplantation.

Methods

Mice. Disruption of *Traf6* expression in TECs was achieved by crossing floxed *Traf6* mice (18) to animals in which a cDNA encoding for the *Cre* recombinase was knocked into the 3′ untranslated region (3′UTR) of the *foxn1* locus (19). The efficiency of deletion through *foxn1*-driven, *Cre*-mediated recombination in both cTECs and mTECs was previously shown to be approximately 80% in the Rosa-26-YFP reporter mice (19). *Traf6$^{fl/fl}$/foxn1-Cre* (*Traf6*ΔTEC) mice were backcrossed for 8 generations to the C57BL/6 background. Heterozygous mouse breeding allowed for the use of littermates as WT controls. *Rag1$^{-/-}$* mice were obtained from the Jackson Laboratories.

mTEC purification. Thymi from *Traf6*ΔTEC and WT mice were dispersed, and single–epithelial cell suspensions were enriched using a Percoll gradient as described previously (24). TEC fractions were treated with anti-CD16/CD32 blocking antibody (BD) and incubated with anti-CD45–PE (30-F11; eBioscience), anti-MHCII–allophycocyanin (M5/114.15.2; eBioscience), biotinylated UEA (Vector Laboratories), streptavidin-PerCP (BD), and/or AIRE-FITC (5H12; provided by H.S. Scott, Walter and Eliza Hall Institute of Medical Research, Melbourne, Australia) antibodies. Multiparameter analysis of stained cell suspensions were performed on an LSR II flow cytometer (BD) at Icahn School of Medicine at Mount Sinai Flow Cytometry Shared Resource Facility and analyzed with FlowJo software (TreeStar Inc.).

AIH histopathology. For assessment of liver inflammation, the left liver lobe from *Traf6*ΔTEC and WT mice was excised, fixed in 10% formalin, and embedded in paraffin. Liver sections were stained with H&E. AIH was evaluated by a liver pathologist and scored using light microscopy and a modified Scheuer scoring scale (62, 63), assigning scores for portal inflammation (0, normal; 1, mild — sprinkling of cells in portal tracts; 2, moderate — lymphoid aggregates in some portal tracts; 3, severe — lymphoid aggregates in most portal tracts), interface hepatitis (0, none; 1, mild — focal, present in few portal tracts; 2, moderate — focal in most portal tracts or continuous in few portal tracts; 3, severe — continuous in most portal tracts), and lobular inflammation (0, none; 1, mild — scattered foci of lobular-infiltrating lymphocytes; 2, moderate — numerous foci of lobular-infiltrating lymphocytes; 3, severe — extensive pan–lobular-infiltrating lymphocytes).

ALT levels. ALT levels were detected by reflectance spectrophotometry using the VITROS ALT Slides and the VITROS Chemistry Products Calibrator Kit 3 on VITROS 250/350/950 and 5,1 FS Chemistry Systems and the VITROS 5600 Integrated System at Icahn School of Medicine at Mount Sinai Chemistry, ENDO and STAT Shared Resource Facility.

Quantitative assessment of fibrosis. Paraffin-embedded liver sections were stained with picrosirius red to measure collagen content as described previously (64), and a Bioquant computerized morphometry program was used to quantify staining intensity. Assessment of collagen staining was obtained by birefringence microscopy using an Axioplan II microscope (Carl Zeiss Inc.) at Icahn School of Medicine at Mount Sinai Microscopy Shared Resource Facility. Each staging of fibrosis was assessed in 10–30 fields at ×100 magnification, and the average was calculated for each mouse.

Immunostaining. For immunofluorescence staining, frozen thymic or liver sections were fixed in ice-cold acetone. Sections were incubated in 1% H_2O_2 in PBS for 5 minutes, blocked in 10% egg white and 0.5% BSA in PBS, washed in 0.05% Tween in PBS, and incubated in 2 μg/ml UEA conjugated to biotin (Vector Laboratories) or AIRE (M-300; Santa Cruz Biotechnology Inc.), K5 (AF138; Covance), K8 (TROMA-1; provided by Developmental Studies Hybridoma Bank, University of Iowa), TRAF6 (H-274; Santa Cruz Biotechnnology Inc.), CD3 (Dako Cytomation), CD4 (H129.19; BD), and CD8 (53-6.7; BD) antibodies for 2 hours at room temperature. Imaging was performed using anti-rat Alexa Fluor 488, anti-rabbit Alexa Fluor 488, or Alexa Fluor 594 (Invitrogen), and streptavidin-rhodamine (Jackson Immunoresearch Laboratories) secondary fluorescent antibodies. All images were acquired with an Axioplan II microscope (Carl Zeiss Inc).

Flow cytometry. Single-cell suspensions of thymi and peripheral lymph nodes were prepared by mechanical dispersion. Various tissues from perfused mice were homogenized, and lymphocyte populations were isolated on a 40%/70% Percoll (GE Healthcare) gradient as previously described (33). Cell suspensions were incubated with anti-CD16/CD32 blocking antibody (BD) for 10 minutes and stained with the corresponding antibody mixtures on ice. The following monoclonal antibodies were used (from eBioscience, unless otherwise indicated): CD138-biotin (281.2; BD); NK1.1-biotin (PK136; BD); CD25-FITC (7D4; BD); CD3ε-FITC (145-2C11); CD69-FITC (H1.2F3; BD); CD44-PE (IM7; BD); PE-streptavidin; CD4-PerCP (LT34); CD8a-PerCP (53-6.7; BD); CD4–PE-Cy7 (GK1.5); steptavidin–PE-Cy7; CD3ε–PerCP-Cy5.5 (145-2C11); CD4-allophycocyanin (L3T4; BD); CD62L-allophycocyanin (MEL-14); MHCII-allophycocyanin (M5/114/15.2); CD8a–Pacific Blue (53-6.7); CD45–Alexa Fluor 750 (30-F11); CD19–eFluor 450 (eBio1D3); FOXP3-PE (FJK-16s). Intracellular staining for FOXP3 was performed with the anti-mouse/rat FOXP3 staining antibody set (eBioscience) and cytofix/cytoperm kit (BD). Intracellular cytokine staining was performed with anti–IL-4–PE (BD), anti–IL-17A–PE-Cy7 (BD), and anti–IFN-γ–allophycocyanin (BD) after cells had been stimulated in vitro for 6 hours with Leukocyte Activation Cocktail and GolgiPlug (BD) according to the manufacturer's instructions. Multiparameter analysis of stained cell suspensions was performed on an LSR II flow cytometer (BD) and analyzed with FlowJo software (TreeStar Inc.).

Autoantibodies and plasma cells. The presence of autoantibodies in the sera of *Traf6*ΔTEC and control mice were analyzed by incubating frozen sections of tissues derived from *Rag1*$^{-/-}$ mice with sera (1:40 dilution) from different animals, followed by FITC-labeled anti–mouse IgG secondary antibody and fluorescent microscopy. Serum ANAs were detected using HEp-2 cells fixed on glass slides (MBL BION) according to the manufacturer's protocol. Anti-SMA, anti-LKM, and anti-SLA autoantibodies were analyzed in sera of *Traf6*ΔTEC and WT mice by mouse-specific ELISA kits (Glory Science Co.; BlueGene Biotech). All samples were run in duplicates. ELISA plates were read on a μQuant Microplate Reader (Bio-Tek Instruments Inc.). Plasma cells were detected by staining paraffin-embedded liver sections with methyl green-pyronin (Sigma-Aldrich). The severity of plasma cell infiltration was based on an estimate of the proportion of plasma cells in the inflammatory infiltrate, as follows: 0, none; 1, occasional plasma cells; 2, moderate plasma cells (<30%); 3, severe plasma cells (>30%, or occurring in sheets or clusters). All images were acquired with an Axioplan II microscope (Carl Zeiss Inc.).

Serum Ig and cytokine measurements. Total Ig and serum Ig isotypes were determined with a commercial ELISA kit (SouthernBiotech) using 1:500 serum dilutions. All samples were run in triplicates. ELISA plates were read on a μQuant Microplate Reader (Bio-Tek Inc.). Serum cytokine levels were determined using a Cytometric Bead Array (CBA; BD) cytokine kit according to the manufacturer's instructions. Samples were collected on an LSR Fortessa cytometer (BD) and analyzed with FCAP Array software (Soft Flow Inc.). TGF-β and IL-10 protein and RNA levels were quantified by ELISA and real-time quantitative PCR kits, respectively. All samples were run in triplicates. ELISA plates were read on a μQuant Microplate Reader (Bio-Tek Instruments Inc.). RNA was isolated with RNeasy Mini Kit (Qiagen) as described by the manufacturer. RNA (1 μg) was used to generate cDNA using a Clontech cDNA Synthesis Kit. mRNA was quantified with a LightCycler 480 thermocycler (Roche). Transcript abundance was normalized to that of mRNA encoding GAPDH. IL-10 and TGF-β were quantified in liver lysates with mouse-specific ELISA kits (BD; Roche).

Western blots. Tissue samples were homogenized on ice in lysis buffer containing 50 mM Tris (pH 8.0), 150 mM NaCl, 1% NP-40, 10% glycerol, and a protease/phosphatase inhibitor cocktail (Roche). Lysates were clarified by centrifugation, and supernatants were mixed with SDS Laemmli buffer, separated by SDS-PAGE, and visualized by Western blot. Protein blots were blocked with 5% nonfat dried milk in PBS for 1 hour, washed with PBS with 0.05% Tween20, and incubated for 1 hour in a 1:100 dilution of sera from individual *Traf6*ΔTEC or WT mice. After washing with PBS with Tween20, blots were incubated with anti–mouse IgG–horseradish peroxidase (1:2,000; GE Healthcare) for 1 hour, and protein bands were revealed with a chemiluminescence reagent (Western Lightning; PerkinElmer).

In vitro suppression and iTreg induction assays. Sorted $CD4^+CD8^-CD25^-$ T cells (5×10^4) were cultured with irradiated splenocytes (5×10^4), stimulated with 1 μg/ml plate-bound anti-CD3ε (eBioscience), and labeled with CFSE (5 μM; Molecular Probes) in the presence or absence of $CD4^+CD8^-$

$CD25^+$ Tregs at the indicated ratios. After 72 hours, cultured cells were stained with anti-CD4–PE-Cy7 (GK1.5; eBioscience) antibody, and proliferating $CD4^+CFSE^+$ T cells were assessed by flow cytometry. For induction of iTregs, sorted $CD4^+CD8^-CD25^-$ T cells (5×10^4) were cultured in the presence of anti-CD3 antibody (1 μg/ml), 10 ng/ml mouse recombinant IL-2 (BD), and 5 ng/ml human recombinant TGF-β (eBioscience) for 4 days. Analysis of iTregs was performed by staining with anti-CD4–PE-Cy7 (GK1.5; eBioscience), anti-CD25–FITC (7D4; BD), and anti-FOXP3–PE (FJK-16s; eBioscience) antibodies and flow cytometry. All samples were run in triplicates, collected on an LSR II flow cytometer (BD), and analyzed with FlowJo software (TreeStar Inc.).

Mixed lymphocyte reactions. Hematopoietic cells were isolated from various tissues of *Traf6*ΔTEC or WT mice using a Percoll gradient. Total cells were then incubated with CD11c-coupled MicroBeads (Miltenyi Biotec) and passed through magnetic columns for positive selection of APCs. The flow-through was collected, incubated with a biotin cocktail followed by anti-biotin-coupled MicroBeads (Miltenyi Biotec), and once again passed through magnetic columns for negative selection of T cells. Total $CD4^+$ T cells were counted and stained with CFSE. Allogeneic or syngeneic liver and spleen, and syngeneic lung and kidney, $CD11c^+$ cells were plated with $CD4^+$ T cells (1:1 ratio) in a 96-well flat-bottom plate for 72 hours. DCs (1×10^5, unloaded or loaded with lysates) were cocultured with $CD4^+$ T cells (1×10^5) in a U-bottom 96-well tissue plate for 5 days. 10 ng/ml mouse recombinant IL-2 (BD) was added to the culture after 3 days. All samples were run in triplicates. Proliferation of $CD4^+$ T cells was analyzed by CFSE dilution on an LSR II flow cytometer (BD).

Generation of DCs. Bone marrow–derived DCs were generated after 5 days of culture with GM-CSF supernatant purified from J558 cells (ATCC) grown in RPMI1640 (Invitrogen) supplemented with 10% FBS (HyClone) and 1% antibiotic-antimycotic solution (Invitrogen) at 37°C in a 5% CO_2 atmosphere.

Preparation of lysates. Whole-cell extracts were resuspended in serum-free medium and subjected to 4 freeze-thaw cycles by alternating between dry ice and 37°C. The lysate was centrifuged for 10 minutes at 300 *g* to remove debris, and the supernatant was collected. The protein concentration of the lysate was determined by a commercial assay (Bio-Rad). The lysate was added to DCs at a final concentration of 100 μg protein/ml.

Adaptive transfer into Rag1$^{-/-}$ recipients. 2.5×10^5 sorted liver or spleen $NK1.1^-CD3^+$ T cells, or liver $NK1.1^-CD3^+CD4^+$ or $NK1.1^-CD3^+CD8^+$ T cells, isolated from *Traf6*ΔTEC or control mice were intravenously injected into *Rag1*$^{-/-}$ recipient mice. Sera isolated from *Traf6*ΔTEC or WT mice were intravenously injected into *Rag1*$^{-/-}$ recipient mice. Mice were sacrificed approximately 6 weeks after adoptive transfer, and liver samples were fixed in 10% buffered formalin. Paraffin-embedded sections were stained with H&E and analyzed by light microscopy. Histopathological scoring was performed by a liver pathologist as described above.

Statistics. *Traf6*ΔTEC and WT samples were compared by 2-tailed Student's *t* test (Excel; Microsoft Inc.). A *P* value less than 0.05 was considered significant.

Study approval. Animals were housed in specific pathogen–free conditions and were used and maintained in accordance with institutional guidelines. Animal protocols were approved by the IACUC of the Icahn School of Medicine at Mount Sinai.

Acknowledgments

The authors thank Andrea D. Branch and Arielle Klepper for protocols and advice, Scott L. Friedman and Andrea D. Branch for critically reading the manuscript, Nancy R. Manley for providing *foxn1-Cre* knockin mice, and Marie E. Grace for advice and technical support with serum biochemical analysis. A.J. Bonito was supported by Icahn School of Medicine at Mount Sinai's Immunology Institute training T32 AI007605-09 grant and by R01 grant AI068963-01. C. Aloman was supported by grant 1K08DK088954. E.G. Weinstein was supported by R01 grants AI088106-01 and AI068963-01. This work was supported by NIAID grants R01 AI49387-01, R56 AI049387-05, and R01 AI068963-01.

Received for publication June 19, 2012, and accepted in revised form May 17, 2013.

Address correspondence to: Konstantina Alexandropoulos, Icahn School of Medicine at Mount Sinai, One Gustave L. Levy Place, Box 1089, New York, New York 10029, USA. Phone: 212.659.8610; Fax: 212.987.5593; E-mail: k.alexandropoulos@mssm.edu.

1. Nitta T, Murata S, Ueno T, Tanaka K, Takahama Y. Thymic microenvironments for T-cell repertoire formation. *Adv Immunol*. 2008;99:59–94.
2. Klein L, Hinterberger M, Wirnsberger G, Kyewski B. Antigen presentation in the thymus for positive selection and central tolerance induction. *Nat Rev Immunol*. 2009;9(12):833–844.
3. Anderson MS, et al. Projection of an immunological self shadow within the thymus by the aire protein. *Science*. 2002;298(5597):1395–1401.
4. Derbinski J, Schulte A, Kyewski B, Klein L. Promiscuous gene expression in medullary thymic epithelial cells mirrors the peripheral self. *Nat Immunol*. 2001;2(11):1032–1039.
5. Tykocinski LO, Sinemus A, Kyewski B. The thymus medulla slowly yields its secrets. *Ann N Y Acad Sci*. 2008;1143:105–122.
6. Alexandropoulos K, Danzl NM. Thymic epithelial cells: antigen presenting cells that regulate T cell repertoire and tolerance development. *Immunol Res*. 2012;54(1–3):177–190.
7. Aschenbrenner K, et al. Selection of Foxp3+ regulatory T cells specific for self antigen expressed and presented by Aire+ medullary thymic epithelial cells. *Nat Immunol*. 2007;8(4):351–358.
8. Apostolou I, Sarukhan A, Klein L, von Boehmer H. Origin of regulatory T cells with known specificity for antigen. *Nat Immunol*. 2002;3(8):756–763.
9. Jordan MS, et al. Thymic selection of CD4+CD25+ regulatory T cells induced by an agonist self-peptide. *Nat Immunol*. 2001;2(4):301–306.
10. Irla M, Hollander G, Reith W. Control of central self-tolerance induction by autoreactive CD4+ thymocytes. *Trends Immunol*. 2010;31(2):71–79.
11. Burkly L, et al. Expression of relB is required for the development of thymic medulla and dendritic cells. *Nature*. 1995;373(6514):531–536.
12. Akiyama T, et al. Dependence of self-tolerance on TRAF6-directed development of thymic stroma. *Science*. 2005;308(5719):248–251.
13. Kajiura F, et al. NF-kappa B-inducing kinase establishes self-tolerance in a thymic stroma-dependent manner. *J Immunol*. 2004;172(4):2067–2075.
14. Boehm T, Scheu S, Pfeffer K, Bleul CC. Thymic medullary epithelial cell differentiation, thymocyte emigration, and the control of autoimmunity require lympho-epithelial cross talk via LTbetaR. *J Exp Med*. 2003;198(5):757–769.
15. Akiyama T, et al. The tumor necrosis factor family receptors RANK and CD40 cooperatively establish the thymic medullary microenvironment and self-tolerance. *Immunity*. 2008;29(3):423–437.
16. Mathis D, Benoist C. Aire. *Annu Rev Immunol*. 2009; 27:287–312.
17. Akirav EM, Ruddle NH, Herold KC. The role of AIRE in human autoimmune disease. *Nat Rev Endocrinol*. 2011;7(1):25–33.
18. Kobayashi T, et al. TRAF6 is a critical factor for dendritic cell maturation and development. *Immunity*. 2003;19(3):353–363.
19. Gordon J, et al. Specific expression of lacZ and cre recombinase in fetal thymic epithelial cells by multiplex gene targeting at the Foxn1 locus. *BMC Dev Biol*. 2007;7:69.
20. Manley NR, Condie BG. Transcriptional regulation of thymus organogenesis and thymic epithelial cell differentiation. *Prog Mol Biol Transl Sci*. 2010;92:103–120.
21. Farr AG, Anderson SK. Epithelial heterogeneity in the murine thymus: fucose-specific lectins bind medullary epithelial cells. *J Immunol*. 1985;134(5):2971–2977.
22. Gray D, Abramson J, Benoist C, Mathis D. Proliferative arrest and rapid turnover of thymic epithelial cells expressing Aire. *J Exp Med*. 2007;204(11):2521–2528.
23. Rossi SW, et al. RANK signals from CD4(+)3(–) inducer cells regulate development of Aire-expressing epithelial cells in the thymic medulla. *J Exp Med*. 2007;204(6):1267–1272.
24. Danzl NM, Donlin LT, Alexandropoulos K. Regulation of medullary thymic epithelial cell differentiation and function by the signaling protein Sin. *J Exp Med*. 2010;207(5):999–1013.
25. Czaja AJ. Animal models of autoimmune hepatitis. *Expert Rev Gastroenterol Hepatol*. 2010;4(4):429–443.
26. Mieli-Vergani G, Vergani D. Autoimmune hepatitis. *Nat Rev Gastroenterol Hepatol*. 2011;8(6):320–329.
27. Krawitt EL. Autoimmune hepatitis. *N Engl J Med*. 2006;354(1):54–66.
28. Homberg JC, et al. Chronic active hepatitis asso-

ciated with antiliver/kidney microsome antibody type 1: a second type of "autoimmune" hepatitis. *Hepatology*. 1987;7(6):1333–1339.
29. Martini E, Abuaf N, Cavalli F, Durand V, Johanet C, Homberg JC. Antibody to liver cytosol (anti-LC1) in patients with autoimmune chronic active hepatitis type 2. *Hepatology*. 1988;8(6):1662–1666.
30. Czaja AJ. Autoantibodies as prognostic markers in autoimmune liver disease. *Dig Dis Sci*. 2010; 55(8):2144–2161.
31. Baeres M, et al. Establishment of standardised SLA/LP immunoassays: specificity for autoimmune hepatitis, worldwide occurrence, and clinical characteristics. *Gut*. 2002;51(2):259–264.
32. Czaja AJ, Shums Z, Norman GL. Frequency and significance of antibodies to soluble liver antigen/liver pancreas in variant autoimmune hepatitis. *Autoimmunity*. 2002;35(8):475–483.
33. Czaja AJ, Donaldson PT, Lohse AW. Antibodies to soluble liver antigen/liver pancreas and HLA risk factors for type 1 autoimmune hepatitis. *Am J Gastroenterol*. 2002;97(2):413–419.
34. Kanzler S, et al. Clinical significance of autoantibodies to soluble liver antigen in autoimmune hepatitis. *J Hepatol*. 1999;31(4):635–640.
35. Ballot E, Homberg JC, Johanet C. Antibodies to soluble liver antigen: an additional marker in type 1 autoimmune hepatitis. *J Hepatol*. 2000;33(2):208–215.
36. Krawitt EL. Discrimination of autoimmune hepatitis: autoantibody typing and beyond. *J Gastroenterol*. 2011;1:39–41.
37. Anderson MS, Venanzi ES, Chen Z, Berzins SP, Benoist C, Mathis D. The cellular mechanism of Aire control of T cell tolerance. *Immunity*. 2005; 23(2):227–239.
38. Parel Y, Chizzolini C. CD4+ CD8+ double positive (DP) T cells in health and disease. *Autoimmun Rev*. 2004;3(3):215–220.
39. Parel Y, Aurrand-Lions M, Scheja A, Dayer JM, Roosnek E, Chizzolini C. Presence of CD4+CD8+ double-positive T cells with very high interleukin-4 production potential in lesional skin of patients with systemic sclerosis. *Arthritis Rheum*. 2007; 56(10):3459–3467.
40. Pahar B, Lackner AA, Veazey RS. Intestinal double-positive CD4+CD8+ T cells are highly activated memory cells with an increased capacity to produce cytokines. *Eur J Immunol*. 2006;36(3):583–592.
41. Xie D, et al. Peripheral CD4+CD8+cells are the activated T cells expressed granzyme B (GrB), Foxp3, interleukin 17 (IL-17), at higher levels in Th1/Th2 cytokines. *Cell Immunol*. 2009;259(2):157–164.
42. Czaja AJ, Manns MP. Advances in the diagnosis, pathogenesis, and management of autoimmune hepatitis. *Gastroenterology*. 2010;139(1):58–72.e54.
43. Longhi MS, Ma Y, Mieli-Vergani G, Vergani D. Aetiopathogenesis of autoimmune hepatitis. *J Autoimmun*. 2010;34(1):7–14.
44. Ichiki Y, Aoki CA, Bowlus CL, Shimoda S, Ishibashi H, Gershwin ME. T cell immunity in autoimmune hepatitis. *Autoimmun Rev*. 2005;4(5):315–321.
45. Derbinski J, Pinto S, Rosch S, Hexel K, Kyewski B. Promiscuous gene expression patterns in single medullary thymic epithelial cells argue for a stochastic mechanism. *Proc Natl Acad Sci U S A*. 2008; 105(2):657–662.
46. King CG, et al. TRAF6 is a T cell-intrinsic negative regulator required for the maintenance of immune homeostasis. *Nat Med*. 2006;12(9):1088–1092.
47. Peiseler M, et al. FOXP3+ regulatory T cells in autoimmune hepatitis are fully functional and not reduced in frequency. *J Hepatol*. 2012;57(1):125–132.
48. Lan Q, Fan H, Quesniaux V, Ryffel B, Liu Z, Zheng SG. Induced Foxp3(+) regulatory T cells: a potential new weapon to treat autoimmune and inflammatory diseases? *J Mol Cell Biol*. 2012;4(1):22–28.
49. Zhou X, et al. Therapeutic potential of TGF-beta-induced CD4(+) Foxp3(+) regulatory T cells in autoimmune diseases. *Autoimmunity*. 2011;44(1):43–50.
50. Calne RY, et al. Induction of immunological tolerance by porcine liver allografts. *Nature*. 1969; 223(5205):472–476.
51. Qian S, Demetris AJ, Murase N, Rao AS, Fung JJ, Starzl TE. Murine liver allograft transplantation: tolerance and donor cell chimerism. *Hepatology*. 1994;19(4):916–924.
52. Kamada N. The immunology of experimental liver transplantation in the rat. *Immunology*. 1985; 55(3):369–389.
53. Crispe IN. Hepatic T cells and liver tolerance. *Nat Rev Immunol*. 2003;3(1):51–62.
54. Hardtke-Wolenski M, Jaeckel E. Mouse models for experimental autoimmune hepatitis: limits and chances. *Dig Dis*. 2010;28(1):70–79.
55. Donaldson PT. Genetics of liver disease: immunogenetics and disease pathogenesis. *Gut*. 2004; 53(4):599–608.
56. Czaja AJ, Donaldson PT. Genetic susceptibilities for immune expression and liver cell injury in autoimmune hepatitis. *Immunol Rev*. 2000;174:250–259.
57. Donaldson PT. Genetics in autoimmune hepatitis. *Semin Liver Dis*. 2002;22(4):353–364.
58. Ma Y, et al. Antibodies to conformational epitopes of soluble liver antigen define a severe form of autoimmune liver disease. *Hepatology*. 2002; 35(3):658–664.
59. Lankisch TO, Jaeckel E, Strassburg CP. The autoimmune polyendocrinopathy-candidiasis-ectodermal dystrophy or autoimmune polyglandular syndrome type 1. *Semin Liver Dis*. 2009;29(3):307–314.
60. Strassburg CP. Autoimmune hepatitis. *Best Pract Res Clin Gastroenterol*. 2010;24(5):667–682.
61. Christen U, Hintermann E, Jaeckel E. New animal models for autoimmune hepatitis. *Semin Liver Dis*. 2009;29(3):262–272.
62. Scheuer PJ. Classification of chronic viral hepatitis: a need for reassessment. *J Hepatol*. 1991;13(3):372–374.
63. Ward SC, Schiano TD, Thung SN, Fiel MI. Plasma cell hepatitis in hepatitis C virus patients post-liver transplantation: case-control study showing poor outcome and predictive features in the liver explant. *Liver Transpl*. 2009;15(12):1826–1833.
64. Safadi R, et al. Immune stimulation of hepatic fibrogenesis by CD8 cells and attenuation by transgenic interleukin-10 from hepatocytes. *Gastroenterology*. 2004;127(3):870–882.